Optimized thermal envelope of low-income dwellings in Santiago de Chile incorporating *Pinus radiata* wood impregnated with phase change materials

Andrés Tapia Calderón[1], Dieter Boer[2], Carlos Salinas-Lira[3], Diego A. Vasco[1]

[1] Departamento de Ingeniería Mecánica, Universidad de Santiago de Chile (USACH), Av. Lib. Bdo. O'Higgins 33 63 – Estación Central, Santiago de Chile, Chile, e-mail: diego.vascoc@usach.cl

[2] Departament d'Enginyeria Mecànica, Universitat Rovira i Virgili, Av. Paisos Catalans 26, 43007 Tarragona, Spain, e-mail: dieter.boer@urv.cat

[3] Departamento de Ingeniería Mecánica, Universidad del Bío Bío, Av. Collao 1202 – Concepción, Bío Bío, Chile, e-mail: casali@ubiobio.cl

Keywords: *Retrofit, Phase change materials, Multi-objective optimization, Energy poverty*

Abstract

The demand for air conditioning and heating in the construction sector has increased in about two decades, mainly because of demographic and economic growth. The result of this increase in energy consumption has been more greenhouse gas emissions (GHGs). This paper proposes a multi-objective optimization design that helps reduce heating, ventilation, and air-conditioning (HVAC) energy consumption and increases the thermal comfort levels in low-income housing. Achieving these objectives required choosing a dwelling unit that is representative of the Chilean housing stock, which was identified with the help of the National Housing Monitoring Network (ReNaM). The selected optimization variables correspond to the type of windows, type and thickness of ceiling insulation, and type of PCM-impregnated Pinus radiata wood panel, with PCM melting points between 8 and 27 °C. Subsequently, we minimized the hours of thermal discomfort and the dwelling typology's electrical consumption of heating and cooling

by using the algorithm the Non-dominated Sorting Genetic Algorithm-II (NSGA-II). The main results include a reduction of up to 21.5% in the thermal discomfort hours and a decrease of up to 80.5% in energy consumption associated with the optimal housing typology compared to the base case. Additionally, the economic analysis indicated the payback period is 12.9 years for the Pareto solution, which presents a lower distance to the utopic point (UP).

List of Abbreviations

A	Area [m^2]
C_P	Heat capacity [J/(kg K)]
CV	Coefficient of variation
DM	Decision maker
E	Thermal property
f	Objective function
GA	Genetic algorithm
h	Enthalpy [kJ/kg]
IRR	Internal rate of return
k	Thermal conductivity [W/(m K)]
L	Latent heat [kJ/kg]
M	Measured quantity
M1	West-facing walls of Bedroom 1 and living room
M2	North-facing walls of Bedrooms 1 and 2
M3	East-facing walls of Bedrooms 2 and 3

MDE	Mean deviation of the error
MD	Minimum discomfort hours
ME	Minimum electricity consumption
MOP	Multi-objetive optimization problem
N	Number of values
PBP	Payback period
PCM	Phase change material
P_{PCM}	Price of PCM [USD/kg]
P_W	Price of wood layer per unit of area [USD/m^2]
$P_{W\text{-}PCM}$	Price of the wood layer impregnated with PCM [USD/kg]
PF	Polyester fiber insulation
PNV	Present net value
Q_{PCM}	Mass of PCM [kg]
ReNam	National monitoring network
RMSE	Root mean square error
S	Simulated quantity
SCS	Sustainable construction standard
SSPCM	Shape stabilized phase change material
T	Temperature [°C]

U	Thermal transmittance [W/m^2K]
UP	Utopic point
V	Volume [m^3]
X	Vector of decision variables

Greek symbols

ρ	Density [kg/m^3]
φ	Liquid fraction

Subscript

I	Instant of time
L	Liquid phase
N	Number of decision variables
P	Interval
PC	Phase change
S	Solid phase
W	Wood

Superscript

T	Transpose

1. Introduction

From 1999 to 2019, the world population increased from 6.06 to 7.71 billion (27.2%), and the total energy supply increased from 73,398 to 87,780 PJ (48.2%) during the same period [1]. There is a direct relationship between the share of the population with access to electricity and the gross domestic product (GDP). In those countries with GDP values greater than USD 20,000, all of the population has access to electricity [2]. In recent years, Chile has experienced increases in energy consumption because of the country's economic and demographic growth that involves, at the same time, higher demand for air conditioning and heating [3]. This increase in energy demand brings with it an increase in greenhouse gas emissions (GHGs), which in turn contribute to global warming. In 2016, Chile recorded 1,166,77.5 kt CO_2eq, which is 114.7% higher than the emissions reported in 1990 [4]. In 2020, the residential subsector consumed 56,411.7 GWh, equivalent to 74.5% of the energy consumption of the commercial, public, and residential sectors, representing 23% of the total energy consumption. In the residential sector, the predominant energy sources are biomass (38%), electricity (25%), and liquefied gas (23%) [5]. HVAC and sanitary hot water consume 53% and 20% of these energy sources, respectively [6]. Therefore, Chile's Ministry of Housing and Urban Planning created the Housing Energy Rating in 2012 to provide families with information about the energy efficiency of dwellings, allowing them to make better decisions when buying or renting a house [7]. The Ministry of Housing and Urban Planning has fostered improvements in housing stock thermal efficiency through a subsidy program, which focuses on financial assistance for retrofitting existing dwellings to meet the national thermal regulation. The "Family Equity Protection Program" aims to retrofit social housing with funding ranging from USD 3350 to 4360 to improve walls, ceilings, roofs, and floors and decrease infiltrations [8]. One of the leading solutions to improve the energy performance of buildings is to control the heat flow through the thermal envelope. The function of a building envelope is to separate the interior from the external environment characterized by fluctuations in temperature,

humidity, wind velocity, rainfall, solar radiation, and other environmental factors that affect thermal comfort. Generally, architects and engineers classify the building envelope into opaque and transparent surfaces. Opaque surfaces contain walls, floors, and roofs, while transparent surfaces include windows, skylights, and glass partitions [9]. The thermal envelope prevents heat losses or gains inside the building and controls the solar gains [10].

1.1. Shape-stabilized PCMs (SSPCMs) based on wood

Passive systems take advantage of the thermal energy available in the environment to improve comfort conditions in buildings, reducing the use of active heating and cooling systems [11]. Some types of these systems include the use of ventilated facades [12], increasing the thermal inertia of building elements by incorporating Phase change materials (PCMs) [13], and enhancing free-cooling and night ventilation techniques. PCMs have proven to be appropriate for increasing the thermal inertia of a building, which translates into a reduction of the peak heat flow through walls and an increase in the time delay of heat flow through walls. Five methods are recognized for incorporating PCMs into the building envelope: (a) direct incorporation, (b) immersion, (c) micro-encapsulation and macro-encapsulation, (d) form-stabilized PCMs, and (e) shape-stabilized PCMs (SSPCMs) [14]. SSPCMs can maintain the solid structure's shape in phase change. Physical methods such as mixing, adsorption, and impregnation or chemical methods allow for obtaining SSPCMs. PCMs support materials may include high-density polyethylene, styrene and butadiene, and porous inorganic materials [15]. The salient qualities of SSPCMs are the following: (i) heat capacity comparable with other PCMs, (ii) adequate thermal conductivity, (iii) compatibility with building envelope materials, (iv) the support material can also serve the function of being a structural element of the building envelope, and (v) no coating or lining is required to prevent the flow of PCMs out of the support material [16]. Wood is an attractive alternative for being used as a support material for impregnation since it is a porous material with attractive thermo-physical and mechanical properties. Mathis et al. [17] impregnated two hardwood species, red oak and sugar maple, with a microencapsulated PCM to improve the thermal mass of wood panels for flooring. They found 77% and 7.1% thermal mass

improvements for red oak and sugar maple, respectively. Fernández et al. [18] found that adding microencapsulated PCM in the adhesive does not affect the mechanical qualities of plywood boards, and the thermal mass increases up to 19%. Barreneche et al. [19] studied the thermo-physical and mechanical properties and reaction to fire after impregnating black alder wood with two paraffinic resins (RT-21 and RT-27). They found a latent heat range of 2.41 J/g–20.62 J/g, with weight ratios ranging from 1.5%–29.9%. Temiz et al. [20] impregnated Scots pine (Pinus sylvestris L.) sapwood with a eutectic mixture of capric and stearic acid. They found values of enthalpy and phase change temperature of 94 J/g and 82 J/g, and 22.97 °C and 22.05 °C. Zhao et al. [21] used carbonized wood, impregnated under vacuum with polyethylene glycol as PCM. They compared two samples of different thicknesses and found that the fusion and solidification enthalpies of the thinner sample (0.5 cm) are 120.9 and 132.3 J/g, respectively, whereas for the thicker sample (1 cm), these values are 104.3 and 113.2 J/g, respectively. Ma et al. [22] delignified and then vacuumed impregnated cedar wood with a eutectic capric-palmitic acid mixture. They found that the impregnation ratio of the eutectic PCM mixture in the delignified wood reached 61.2% without leakage. Also, melting temperature of the composite was 23.4 °C, and the melting latent heat was 94.4 J/g. Moreover, the thermal conductivity improved significantly by 133.3%. Fuentes-Sepúlveda et al. [23] thermally characterized Pinus radiata wood, impregnated with octadecane. They found that the composite could reach values of melting enthalpies in 36 to 122 J/g, depending on the PCM load. Montanari et al. [24] prepared a SSPCM with polyethylene glycol/polymethyl methacrylate (PEG/PMMA) and delignified wood as a substrate. The delignified wood showed excellent capacity to absorb the PEG/PMMA polymer blend, and the novel material exhibits a melting and solidification latent heat of 76 and 74 J/g, respectively. Lin et al. [25] fabricated a wood-based thermal storage material (TESW), using an aqueous mixture of PEG and graphene oxide (0.5 wt.%) as impregnated, which the authors refer to as graphene aerogel encapsulated PEG. The authors found that the melting and solidification enthalpy of TESW were 11.81 and 27.91 J/g, respectively. Nevertheless, TESW showed a thermal conductivity increase of 274% when compared with wood. By pressure impregnation, Hartig et al. [26] impregnated spruce, beech,

and poplar wood with a paraffin PCM. The largest levels of PCM per1 m^3 of wood found by the authors were 250 kg for beech, 230 kg for poplar, and 150 kg for spruce. Moreover, PCM-impregnated beech has a melting and solidification latent heat of 23 J/g and 22 J/g, respectively. Despite several works on the characterization of SSPCMs based on wood, to date there are no studies concerning the incorporation of these materials in buildings.

1.2. Improvement of building energy performance with PCMs

Implementing PCMs in the thermal envelope often involves a parametric analysis or optimization. Some standard optimized variables are the PCM phase change temperature, the modified surface(s) or wall(s), and the location of PCM in the envelope. In 2014, Alam et al. [27] studied the potential of a PCM with latent heat of 219 kJ/kg, with different phase change temperatures in a 16 m^2 test room, located in six climate zones in Australia. They noted that the effectiveness of PCM, in terms of energy consumption and average temperature fluctuation reductions, is strongly dependent on local climatic conditions and that no PCM proved to be equally effective over a year. They found that PCM performance depends on local climatic conditions, thermostat setting temperatures, PCM-layer thickness, and surface area. Wang et al. [28] conducted a parametric analysis using EnergyPlus to evaluate the performance of a PCM on the exterior walls of a thermally conditioned enclosure in a building in Shanghai, China. They analyzed the melting temperature of PCM and PCM's thickness and location on the enclosure walls, and they found that the optimum melting temperature of PCM is seasonal, being 24 °C in summer (on the east and west walls) and 22 °C in winter (on the south wall), achieving savings of 28% in the cooling season and 96% in the heating season. Al-Saadi et al. [29] conducted a study wherein they employed simulations of a PCM-enhanced wall of a 167 m^2 one-story house with TRNSYS software, analyzing four U.S. climate zones. They evaluated the performance of PCM at different positions on the exterior walls, closer to the interior, at the center of the panel, and closer to the exterior, and they found that the best configuration was when placing the PCM layer in direct contact with the interior. The results showed savings of 0.8–15.8% in annual cooling loads, depending on the climate, and savings of 4% for heating-

147 dominated climes. Also, the researchers found that the peak cooling load savings ranged from
148 6.8–13.3% and peak heating load savings ranged from 7–10.5%. Implementing PCMs in the
149 thermal envelope of dwellings also considers their effect on thermal comfort aspects. Bohorquez
150 et al. [30] found that a 10 mm thick PCM in the chosen walls results in a maximum thermal
151 stress reduction of 23% when compared with the thermal stress hours in a house without PCM
152 in Santiago de Chile. Ramakrishnan et al. [31] found that a good PCM selection and an
153 improved ventilation design could reduce the thermal discomfort period by 65% in a building
154 located in Melbourne (Australia) during extreme heatwave conditions. Lee and Park [32] found
155 that using PCMs in a traditional Korean house can narrow the comfort PMV range and
156 centralize the optimal point. The design of a house or building requires control over all of the
157 construction variables. The variables that minimize certain objective functions, such as energy
158 consumption, hours of thermal discomfort, initial investment, CO_2 emissions, and operating
159 costs, are commonly optimized. Moreover, before starting a retrofitting project, it is essential to
160 perform an optimal approach to the singularities of the project [33]. These construction
161 variables include the surface ratio between walls and windows, building orientation, insulation
162 levels in walls and roofs, types of windows and glass thickness, shading, thermal envelope
163 materials, and their thicknesses, among others. Gossard et al. [34] optimized the thermal
164 properties of the external walls of a single-story house (112 m^2) located in Nancy (continental
165 weather) and Nice (Mediterranean weather), France. The authors analyzed a single and multi-
166 objective optimization approach to minimize the annual energy consumption and summer
167 comfort degree. The authors used a coupled methodology based on an artificial neural network
168 and NSGA-II. They concluded that multi-objective optimization is a better option, for it ensures
169 that the optimization does not follow a privileged direction. The obtained Pareto fronts of both
170 cities are composed of dispersed optimal solutions. However, higher values of k_{wall} give place to
171 minimum summer comfort degree, and lower values of $(\rho C)_{wall}$ result in maximum annual
172 energy consumption. Asadi et al. [35] used a school building (in Coimbra, Portugal) as a case
173 study to implement multi-objective optimization based on a genetic algorithm and artificial
174 neural network focusing on energy consumption, retrofit cost, and thermal discomfort; as the

175 decision variables in this case were as follows: external wall insulation materials, roof insulation
176 parameters, window type; solar collector type, and HVAC systems. The authors discovered that
177 simultaneous optimization of three objectives yielded a more extensive set of retrofit options,
178 and choosing among them may be difficult.

179 This research sought to contribute to existing knowledge and benefit society by generating a
180 methodology that allows retrofitting of low-income dwellings, using as a base case, i.e., a
181 Chilean house whose thermal records are a part of a public database. The methodology
182 comprises multi-objective optimization to reduce energy consumption and thermal discomfort
183 hours, and it started with validating a house of the National Monitoring Network (ReNaM) that
184 represents the housing stock of the climatic zone of Santiago de Chile. Next, we selected the
185 design variables based on the thermal standard of Chile, comprising the following: type of
186 windows, thermal insulation of walls and ceiling, and, as novelty material, an SSPCM based on
187 *Pinus radiata* wood and commercial PCMs with melting temperature in the range of 8–27 °C.
188 The possibilities for the decision variables obeyed the Chilean national market. Therefore, the
189 optimal results were considered to be more realistic and useful for dwelling owners, retrofitting
190 developers, and policy-makers since the base case and its context met the requirements of
191 government subsidies for energy efficiency projects in low-income dwellings. Subsequently, we
192 minimized the thermal discomfort hours and the housing typology's heating and cooling
193 electricity consumption, using the NSGA-II algorithm for multi-objective optimization.

194 Despite multi-objective optimization having been used before to optimize the thermal envelope
195 of buildings, this research was based on actual data to propose a methodology that can be used
196 in other cases and future applications. Moreover, the analysis of the optimal results based on a
197 utopic point (UP) and decision-maker (DM) point allowed the classification and better analysis
198 of the optimal results. Finally, we performed an economic feasibility analysis by using the
199 chosen Pareto solution with a lower distance to the UP.

200
201
202

2. Methodology

Accurate data concerning thermal comfort and energy consumption to calibrate the computational results are essential to convince house owners and constructors that the methodology results are trustworthy. Figure 1 shows the ten steps of the methodology implemented. First, an analysis of the national housing stock was carried out. Second, a house was selected from the national stock. In the Chilean context, the chosen house belongs to the ReNaM, which contains real-time data on dwellings' external and internal temperature [36]. Third, a housing typology was proposed, taking the characteristics of type of house as the basis. Fourth, the thermal performance of the base case was simulated and calibrated using available data. Fifth, the simulation of the base case was carried out with (active thermal analysis) and without (passive thermal analysis), using HVAC equipment. Sixth, objective functions were set, in this case, thermal discomfort and energy consumption for cooling and heating based on the local market. Seventh, optimization variables were selected for a multi-objective optimization algorithm (NSGA-II). Eighth, an analysis was carried out of the results obtained from the previous step. Ninth, all of the Pareto solutions that correspond to the chosen optimal result were identified and the improvements were compared with the base case. Finally, an economic analysis of the chosen Pareto solution was performed using the present net value (PNV), discounted payback period, and internal rate of return (IRR).

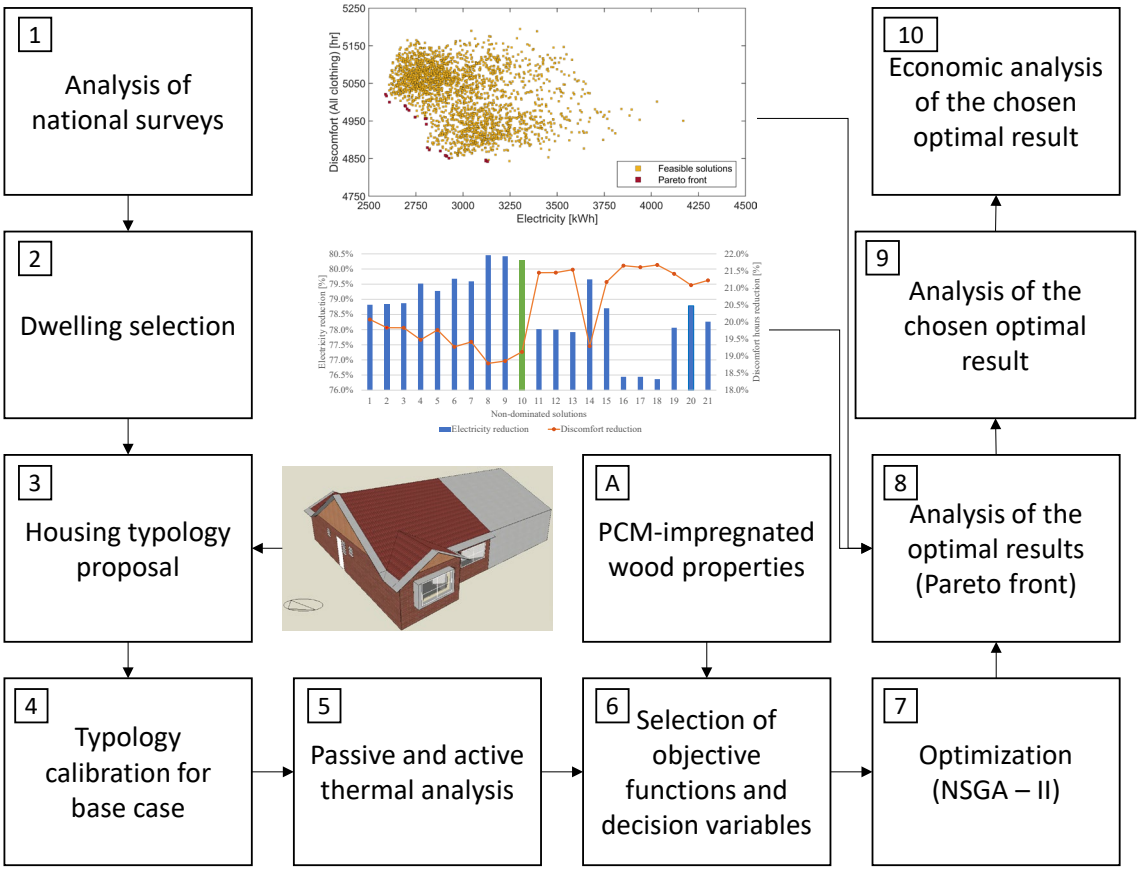

Figure 1. Proposed methodology to reduce thermal discomfort hours and heating and cooling electricity consumption using multi-objective optimization.

3. Base case description

In Chile, thermal zoning is based on the criterion of annual Heating Degree Days (HDDs), and the country's territory is classified into seven thermal zones by using long-standing meteorological information.

The HDDs correspond to the annual sum of the hourly differences between the outdoor air temperature and a base heating temperature for all of the days of the year, considering a baseline temperature of 15 °C (Table 1). Therefore, the heating DGs relate to the energy demand that a dwelling requires to achieve the indoor base temperature. Santiago de Chile (Köppen classification Csa) is located in Thermal Zone 3, characterized by a Mediterranean climate, with moderate temperatures, winters of four to five months with precipitation, and frost increasing toward the south. Intense sunshine in summer, especially in the northeast is another of its

characteristics as is moderate daily temperature oscillation, increasing toward the east and winds mainly from southwest.

Table 1. Annual heating degree days (HDDs) for each thermal zone in Chile.

Thermal zone	HDD (baseline of 15 °C)
1	≤ 500
2	> 500–≤ 750
3	> 750–≤ 1000
4	> 1,000–≤ 1,250
5	> 1,250–≤ 1,500
6	> 1,500–≤ 2,000
7	> 2,000

3.1. Analysis of the Chilean housing stock

According to the 2017 Chilean census [37], the national housing stock comprises 6,486,533 dwellings, of which 79.67% are houses, 17.54% are apartments, and the remaining 2.79% correspond to other types of housing. The National Socioeconomic Characterization (CASEN) 2017 survey [38] distinguishes detached houses, semi-detached houses on one side, semi-detached houses on both sides, and apartments with and without elevators. The Metropolitan region has a more significant number of one-sided semi-detached houses (32%), followed by apartments (28.8%), and detached houses (25.8%). Almost one-third (32%) of the dwellings in Chile was built before 2008 [39]. This aspect is vital, as there have been significant changes in Chilean building regulations during the last 20 years.

249 Regarding floor area, we also reviewed building permits for the same period, finding that for
250 2020, the average floor area of houses and apartments nationwide is 84.14 m^2 and 76.55 m^2,
251 respectively. According to the 2017 census [37], 37.4% of the total housing stock has two
252 bedrooms, followed by 33% of homes with three bedrooms. Regarding the number of
253 occupants, the number of dwellings with 2, 3, and 4 persons amount to 23.9%, 22.8%, and
254 19.1%, respectively. Overcrowding is the ratio between the number of occupants and the
255 number of bedrooms. If this ratio is greater than 2.4, then it is overcrowding according to
256 national standards. In Chile, there is 6.6% of overcrowding.

257 Regarding the exterior wall materials [40], masonry exterior envelopes predominate in the north
258 of Chile from Maule to Arica-Paniracota, while in Ñuble and Biobío regions, there is an even
259 proportion of dwellings with masonry and partition walls, lined on both sides. This scenario
260 changes markedly in the southern regions, from La Araucanía to Magallanes, and dwellings
261 with exterior walls of lighter materials (partition walls lined on both sides) are predominant.
262 Regarding the roof covering material, the predominant roof covering material is zinc, copper, or
263 fiber cement sheeting. The type of floor that prevails in all of Chile's regions corresponds to
264 parquet, floating floor, ceramic tile, carpet, and floor covering. Concerning the energy sources
265 used for heating, more than 60% of dwellings in the northern regions from Arica-Parinacota to
266 Coquimbo do not use any energy source for heating, as these regions are mostly desert and have
267 a dry climate. On the contrary, in the center regions of Valparaíso, the Metropolitan region, and
268 the southern region of Magallanes, the use of natural gas is predominant for heating at 43.5%,
269 50.7%, and 97.3%, respectively. Likewise, firewood and its derivatives have a greater use in the
270 O'Higgins region to the Aysén region. Generally, at the national level, one-story and two-story
271 houses are 74.3%, and 25.5%, respectively. At the national level, 60.8% of homes have some
272 insulation on the roof, and only 26.8% have thermal insulation on the walls. Specifically, 79.1%
273 of the dwellings in Thermal Zone 3 and 53.9% in Thermal Zone 5 have thermal insulation in the
274 roof. Similarly, 15.5% of the dwellings in Thermal Zone 3 and 52.5% in Thermal Zone 5 have
275 thermal insulation in walls. The same report says that 97.3% (4,913,892) of the homes

nationwide use individual stoves or heaters, and 2.4% of the remaining homes (119,369) have central heating. In this same aspect, regarding the use of heating in the home, 90.3% (2,317,338) of the homes in Thermal Zone 3 use heating only in the rooms, while 76.1% (392,151) of the homes in Thermal Zone 5 heat the entire home [41]. At the national level, 67.7% of the dwellings have only one heater, 56.1% in Thermal Zone 3, and 70.5% in Thermal Zone 5. In Thermal Zones 3 and 5, 30% and 27.4% of households have two heaters, respectively. Only 3.1% of homes nationwide have air conditioning equipment, with the most significant presence of this equipment in Thermal Zone 3 (4.6%). On the other hand, in Thermal Zone 5, the number of homes with air conditioning is below the national level at 2.5%.

*3.2. Housing typology calibration: **b**ase case*

Since this work studies the impact of a real retrofitting scenario of a housing typology located in the Metropolitan region of Chile (Csa). The dwelling in the Metropolitan region corresponds to the dwelling coded as NA127, a house located in the Municipality of Macul (Thermal Zone 3). Facing west, semi-detached on one side, one story, with a usable area of between 36 and 70 m^2, built before the year 2000, with exterior walls of heavy material (brick masonry work) and zinc roof covering. This information is used according to Typology 5 of the Chilean standards given in the Residential Characterization Report [6], which has all of the characteristics of Typology 36 identified by Molina et al. [42], except that our housing typology is a semi-detached house.

In detail, Typology 5 is a semi-detached house of the brick structure, with a usable area of 67.7 m^2, ceiling height of 2.4 m, envelope wall area of 51 m^2, roof area of 81.7 $m^{2,}$ and window area of 7.6 m^2. Figures 2a–2c present the views of a one-story house with a usable area of 68.9 m^2. The typology design has been depicted in Figure 2. The interior and exterior doors' dimensions and the distribution of spaces have been modeled according to supreme decree 49 of the Housing and Urban Planning Ministry [42].

To calibrate the proposed NA127 typology, the coefficient of variation of the root mean square error CV(RMSE), and the mean deviation of the error, MDE, are used:

$$CV(RMSE) = \frac{\sqrt{\sum_{i=1}^{N_p}((M_i - S_i)^2/N_p)}}{(\sum_{i=1}^{N_p} M_i)/N_p} \quad (1)$$

$$MDE = \frac{\sum_{i=1}^{N_p}(M_i - S_i)}{\sum_{i=1}^{N_p} M_i} \quad (2)$$

M_i and S_i are the measured and simulated quantities at instant *i,* respectively, and N_p is the number of values in the interval *p*.

The Chilean Housing and Neighborhood Improvement Program: housing, energy, and water efficiency projects [43] seeks to improve the quality of life of families living in urban areas or localities with more than 5,000 inhabitants. This subsidy seeks to improve the housing envelope to reduce its thermal leakage and contribute to improving basic housing services through the efficient use of available natural resources. The subsidy for thermal improvement and thermal efficiency is 170 UF (6,721 USD), and people who own a dwelling whose fiscal appraisal does not exceed 950 UF (37,557.4 USD) can apply. The NA127 housing typology is in a block identified with the ROL number 7069 according to the Chilean tax system [44], where 78.9% of the dwellings meet the criteria of this program.

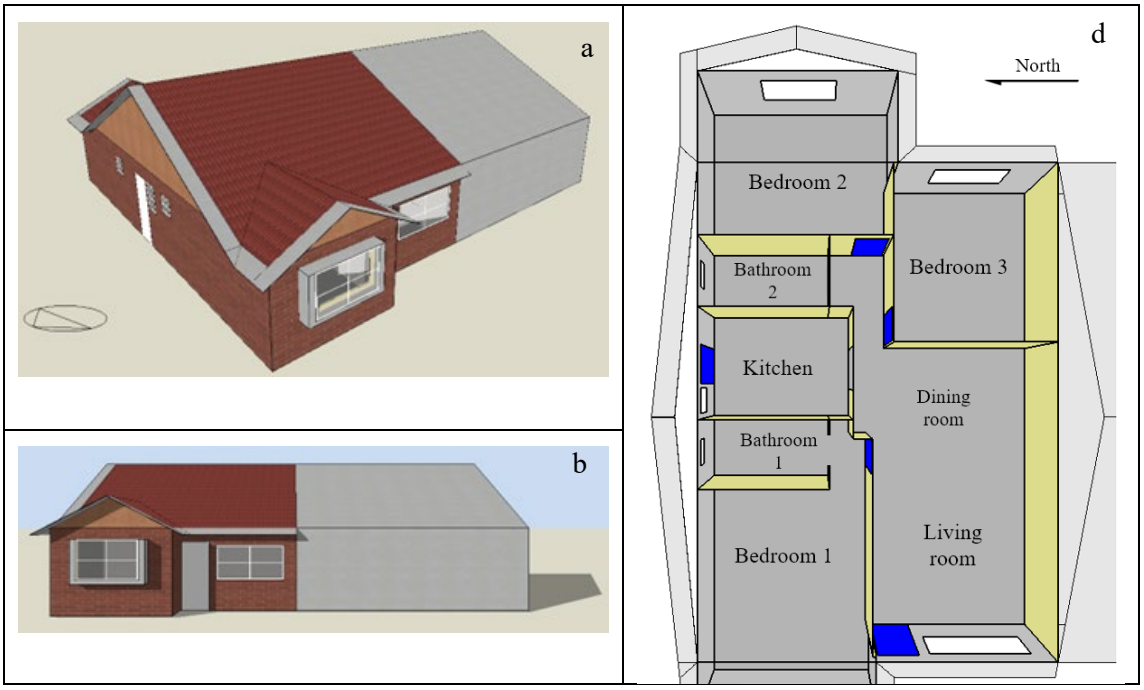

Figure 2. Isometric (a), west (b), east (c), and (d) plan views of the NA127 housing typology.

For monthly data, the ASHRAE 14 guide mentions that a calibrated model has a CV(RMSE) between ± 15% and the MDE between ± 5%, while for hourly data, the range is ± 30% for CV(RMSE) and ± 10% for MDE. Since several essential characteristics of the NA127 house are unknown, such as the configuration of the exterior walls, ceiling and roof, and air infiltrations, as a first approach, we considered construction elements stipulated by Chile's Ministry of Housing and Urban Planning, i.e., the Chile Sustainable Construction Standard (SCS) [45] and NCh853. The details in this regard are in Table 2. Moreover, we assumed a constant air exchange (infiltration and ventilation) of one air renewal per hour for sanitation purposes. The climate file of Santiago de Chile used for the calibration was obtained from the Design-Builder website [46].

Table 2. Construction assembly of the NA127 housing typology according to the Sustainable Construction Standard (SCS) [45].

Construction assembly	**Material**	**ρ $[kg/m^3]$**	**k $[W/(m \cdot K)]$**	**C_p $[J/kg \cdot K]$**	**Thickness $[m]$**	**U $[W/m^2 \cdot K]$**
Exterior walls	Machine made bricks	1920	0.3929	840	0.1400	1.900
Internal partitions	Plasterboard	900	0.25	1000	0.0100	2.040
	Air gap	--	--	--	0.0800	

	Plasterboard	900	0.25	1000	0.0100	
Roof	Zinc board	7690	44.97	418	0.0004	0.468
	Asphalt felt paper	960	0.19	837	0.0010	
	Air gap	--	--	--	variable	
	Glass wool	12	0.04	840	0.0350	
Ceiling	Glass wool	12	0.04	840	0.0350	
	Plasterboard	900	0.25	1000	0.0100	
Pediment	Slotted wood panel	930	0.26	1420	0.0100	
	Asphalt felt paper	960	0.19	837	0.0010	
Floors	Concrete slab	2400	1.63	840	0.1500	3.072
	Ceramic tiles	1900	0.85	840	0.0200	
Exterior doors	Wood	700	0.19	2390	0.0350	2.823
Inner doors	*Plywood*	700	0.15	1420	0.0060	2.500
	Air gap	--	--	--	0.0300	
	Plywood	700	0.15	1420	0.0060	
Windows	Single glass	2500	0.9	840	0.0060	5.778

We first contrasted the external temperature measured by the outdoor sensor of the dwelling with the dry bulb temperature for the validity assessment of the Design-Builder climate file. Figure 3a shows how the external temperatures almost overlap during the typical winter week, except for the maximum temperatures during the last four days, but a similar behavior was noticed. The calibration relies on the internal temperature of ReNaM's NA127 dwelling measured each hour during the typical winter week (19/08–25/08). The first approach gave CV(RMSE) and MDE values of 24.78% and - 17.29%, respectively, which indicates that the proposed typology based on SCS does not represent the actual house (Figure 3b). According to ReNaM's records, House NA127 was built before 2000, and the SCS for houses draws on the thermal regulation updated in 2007. Therefore, we modified two construction assemblies in the energy simulation: the thermal transmittance of the exterior walls, considering machine-made bricks, with values ranging from 1.9 to 3.8 W/m^{2}K, and the air infiltrations ranging from 2.5 to 40 air renewals per hour, according to the baseline established for residential buildings in the Manual of Air Tightness of Buildings in Chile [47]. These ranges were changed to 36 simulations from the one with U = 3.8 W/m^{2}K and 40 air renewals per hour due to air infiltrations representing the lowest CV(RMSE) and MDE values of 16.75 and - 1.08%, respectively (Figure 3c). Further, we eliminated the thermal insulation of the ceiling assembly (Table 2). As a result, the CV(RMSE) rose to 17.93%, and the MDE dropped considerably to 0.0079%. Figure 3d shows how the interior temperature curve of the simulated house with lower thermal insulation conditions better captures the actual house's internal temperature behavior. This precarious insulation condition may explain the poor thermal sensation declared to ReNam by the house's inhabitants during summer and winter.

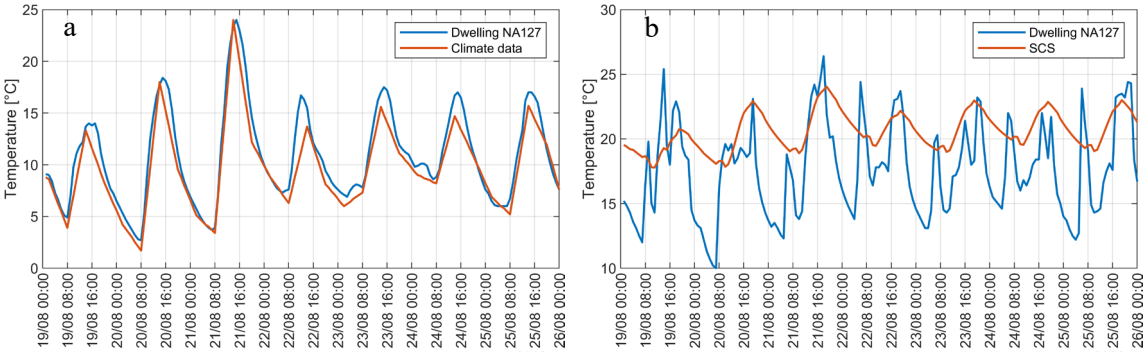

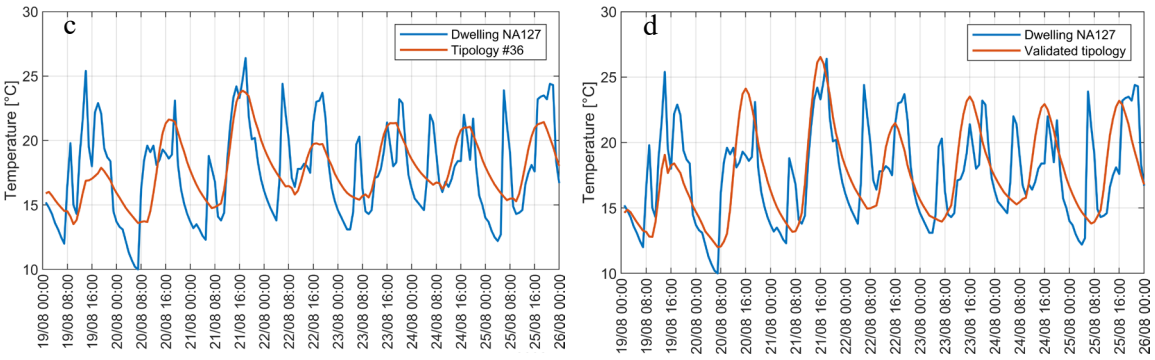

Figure 3. External temperature of dwelling NA127 (a), internal temperature of NA127 housing typology according to SCS (b), considering U_{wall} = 3.8 W/m²K, infiltration rate of 40 air renewals/hour, with (c), and without (d) thermal insulation in the ceiling.

3.3. Passive and active thermal performance analysis of the base case

Passive thermal analysis refers to assessing of thermal comfort of NA127 dwelling without an HVAC system. On the contrary, the active thermal analysis focuses on the energy consumption of a hypothetical HVAC system installed in the NA127 dwelling to maintain comfort levels. The passive analysis of the NA127 dwelling typology was carried out for one year, covering 8760 hours. The thermal discomfort hours, calculated from the method of ASHRAE Standard 55 [48] when the occupants wear winter or summer clothing, were chosen as a parameter for comparing the satisfaction of the occupants of the dwelling. Table 3 summarizes the number of discomfort hours in dwelling rooms during the four seasons. In general, the inhabitant of the dwelling experience 6778.3 hours of thermal discomfort throughout the year, which means that in 22.6% of the period studied, the occupants experienced good thermal comfort. This result of thermal discomfort hours of the base case is high and is like those reported by Lin et al. [49], which ranges between 6350 and 6790. In this work, the authors minimized the life cycle cost and thermal discomfort hours of one single-story concrete residential building in five different Chinese cities of Cfa and Cwa climate.

The active analysis of the calibrated housing typology NA127 contemplates HVAC equipment to determine the heating and cooling demand, considering the thermostat setting temperatures established by the Chile SCS [45]. The conditioned zones of the dwelling are the three

bedrooms, the living room, the dining room, and the kitchen, totaling an area of 60.43 m^2. The HVAC equipment used for each zone corresponds to a PTAC (packaged terminal air conditioner) with electric heating. The HVAC equipment incorporates the following elements: an outside air mixer, a DX cooling coil (direct expansion cooling) with COP of 3, an electric heating coil with 100% efficiency, and a constant volume air supply fan with an efficiency of 90%. Table 4 summarizes the active analysis results for heating and cooling demands.

Table 3. ASHRAE 55 (all clothing) thermal discomfort hours.

Zone	Summer	Autumn	Winter	Spring	Total
	Dec.–Feb.	Mar.–May	Jun.–Aug.	Sep.–Nov.	
Bedroom 1	1906.9	2006.3	2133.3	1941.1	7987.6
Bedroom 2	1428.6	1611.0	1909.8	1552.9	6502.4
Bedroom 3	1493.9	1627.8	1940.9	1538.6	6601.3
Living room, dining room, and kitchen	1599.9	1727.3	1904.7	1637.9	6869.9
Dwelling	1570.1	1699.1	1897.7	1611.3	6778.3

The living room, dining room, and kitchen have the highest heating annual demand (5214.59 kWh) due to the larger area (27.53 m^2), followed by the annual heating demand of bedrooms one, two, and three, with 2889.24, 2409.34, and 1651.22 kWh, respectively. The heating demand intensity of the entire dwelling, which considers only the heated area, is 201.30 kWh/(m^2·year), although Bedroom 2 has the highest demand intensity (241.17 kWh/(m^2·year)), while Bedroom 3 has the lowest (175.47 kWh/(m^2·year)). According to these results, the heating demand intensity of the calibrated base case exceeds 2.84 and 13.45 times the limit value established by the SCS for the Metropolitan region in 2020 (71 kWh/(m^2·year)) and 2050 (15 kWh/(m^2·year)), respectively. Regarding the annual demand for cooling, the living room, dining

386 room, and kitchen present the highest, representing 43% of the total cooling demand.
387 Nevertheless, Bedroom 2 has the highest demand intensity (48.60 kWh/(m^2·year)), while the
388 living room, dining room, and kitchen have the lowest (42.69 kWh/(m^2·year)). Therefore, the
389 cooling demand intensity of the calibrated base case (45.36 kWh/(m^2·year)) exceeds 3.02 and
390 9.07 times the limit value established by the SCS for the Metropolitan region in 2020 (15
391 kWh/(m^2·year)) and 2050 (5 kWh/(m^2·year)), respectively.

392 *Table 4. Annual heating and cooling demands of the NA127 housing typology zones.*

Zone	Heating [kWh]	Cooling [kWh]	Heating [kWh/(m^2·year)]	Cooling [kWh/(m^2·year)]
Bedroom 1	2889.24	641.56	213.86	47.49
Bedroom 2	2409.34	485.54	241.17	48.60
Bedroom 3	1651.22	438.72	175.47	46.62
Living and dining room	5214.59	1175.14	189.41	42.69
Dwelling	12164.38	2740.95	201.30	45.36

393 *3.4. Selection of objective functions and decision variables*

394 The housing typology (base case) shows a precarious condition, i.e., a high amount of thermal
395 discomfort hours and an elevated energy demand for air conditioning. This precarious condition
396 is not uncommon, considering that 32% of dwellings in Chile were built before 2008 [39] when
397 a more rigorous thermal standard did not exist yet. Therefore, we chose the electrical
398 consumption required for heating and cooling and the thermal discomfort hours (ASHRAE 55
399 for all clothing) as minimum objective functions. Both objective functions are opposed to each
400 other since reducing energy consumption implies a reduction in thermal comfort hours.

In Chile, social apartments built with concrete or brick present air infiltrations mainly throughout doors, and windows, giving values in the range of 6–10 air renewals/hour at 50 Pa. Meanwhile, social apartments built with light materials, such as structural panels with steel profiles and envelopes of OSB, fiber cement, or gypsum plasterboard, show higher infiltration rates of 25–30 air renewals/hour due to walls contributing to air infiltration. Dwellings with higher construction standards made of concrete or brick present lower infiltration rates (2.5–4.0 air renewals/hour) [50]. Under this scenario, we decided to perform the optimization process using an air tightness value of 4.0 renovations/hour.

A multi-objective optimization problem (MOP) aims to find a vector of decision variables that satisfies the constraints and optimizes a vector function whose elements represent the objective functions. Equation (3) shows the vector x with n decision variables:

$$x = [x_1, \quad x_2, \quad \dots \quad , x_n]^T \tag{3}$$

Then, the following are objective functions to be minimized or maximized $f(x)$

$$f(x) = [f_1(x), \quad f_2(x), \quad \dots \quad , f_n(x)]^T \tag{4}$$

Since there are several objective functions, the notion of optimum changes since multi-objective problems seeks to find a trade-off, resulting in a set of non-dominated solutions.

Genetic algorithms (GA) have gained popularity in the optimization of building performance thanks to some advantages, such as including continuous variables, discrete variables, suitable for parallel computing, do not “get stuck” in local optima and have a low sensitivity to discontinuities and constraints, making GA very robust algorithms. GA is suitable for solving MOPs since they are population-based and can locate multiple optimal solutions on Pareto fronts. The Design Builder software brings the NSGA-II for conducting multi-objective optimization analysis.

We analyze five decision variables for the base case NA127 housing typology. Three of them correspond to the modification of the exterior walls of the dwelling to meet the following

424 thermal regulations: (i) west-facing walls of Bedroom 1 and the living room (M1), (ii) exterior
425 walls of the north wing of Bedrooms 1 and 2 (M2), and (iii) east-facing exterior walls of
426 Bedrooms 2 and 3 (M3). These modifications consist of a thermal envelope comprising the
427 combination of polyester fiber insulation layers (PF), SSPCM, and plasterboard, as shown in
428 Figure 4. SSPCM uses wood as a support material by using the impregnation process and
429 different phase change temperature PCMs as impregnated. The PCM occupies the wood cell
430 structure, within vessels in hardwood species and the tracheid in softwood species [51]. The
431 combinations result in 129 possible types of exterior walls, and Figure 5 shows the possible wall
432 combinations.

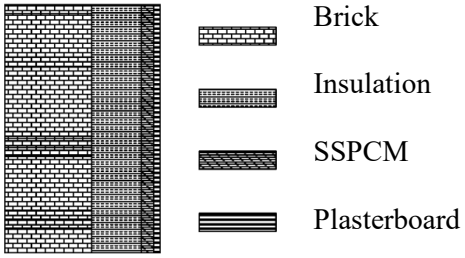

433 *Figure 4. Configuration of the retrofitted exterior walls.*

434 The fourth variable corresponds to the improvement of the roof's thermal insulation,
435 considering that the base case has no thermal insulation. In this case, we consider two insulation
436 options, glass wool insulation of 80 mm thickness and PF of 100 mm thickness. All of these are
437 followed by a layer of 10 mm plasterboard, giving U-values of 0.427 and 0.487 [W/m^{2}K],
438 respectively; both options fulfill the thermal regulations of the roof assembly for the
439 Metropolitan Region. Finally, the window type is the fifth constructive variable to intervene
440 since the base case has single-glazed windows of 6 mm thickness. For the optimization process,
441 six options of window types are available (Table 5).

442 *Table 5. Windows configuration is for the optimization process.*

Windows glazing	Single-clear	Single-clear	Double-transparent	Double-clear	Double-transparent	Double-clear

Glass thickness (mm)	6	6	3	3	6	6
Spacing (mm)	--	--	6	13	6	13
U (W/m^2K)	5.894	5.778	3.159	2.716	3.094	2.665

443 The construction assemblies and windows were chosen based on the feasibility of performing a
444 retrofitting procedure on an existing dwelling in Chile. Considering the five design variables,
445 exploring all of the possible combinations would take about 12.9 million simulations. Therefore,
446 before analyzing the optimization results by implementing Steps 7–10 of the methodology
447 (Figure 1), we explain in the following section the incorporation of PCM-impregnated thermal
448 properties in the simulations with Design Builder.

449

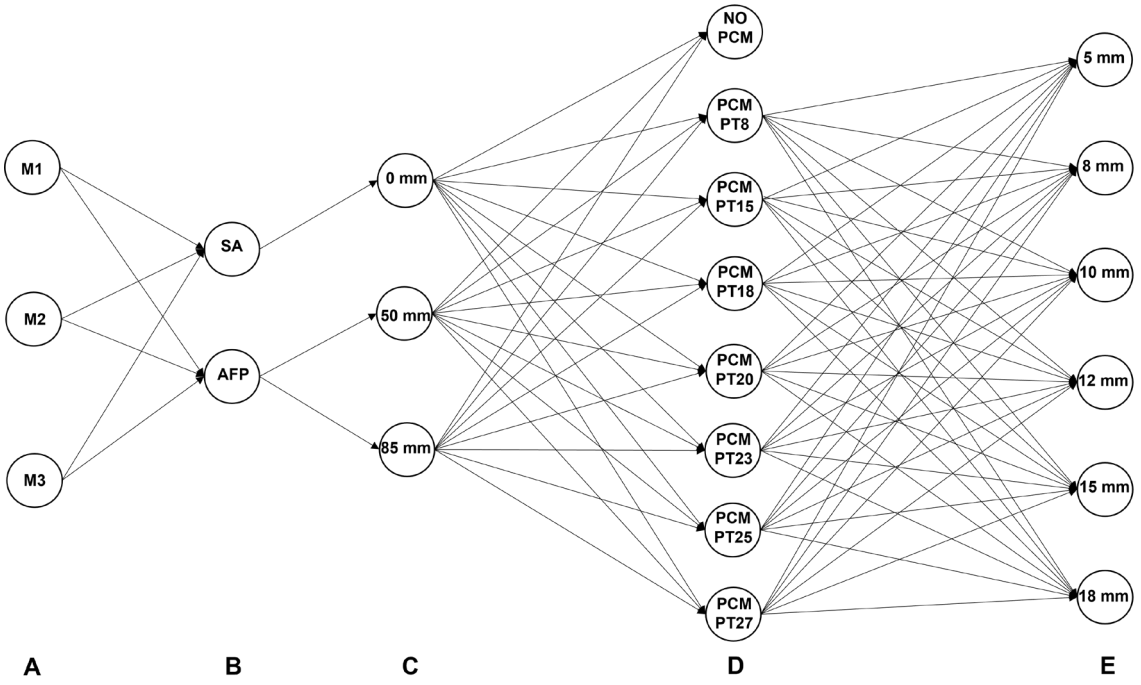

450 *Figure 5. Combinations for walls (A) M1, M2, and M3. (B) Type of thermal insulation, S.A.:*
451 *without insulation, and PF: polyester fiber insulation. (C) The thickness of insulation. (D) Type*
452 *PCM for impregnation. (E) The thickness of the wood layer impregnated with PCM.*

3.4.1. Thermal properties of PCM impregnated Pinus radiata Wood

We used the rule of mixtures (5) and the volume fraction (6) to estimate the thermal properties of impregnated *Pinus radiata* wood with different PCMs. Moreover, we assessed the feasibility of using the rule of mixtures by calculating the relative error of the predicted thermal conductivity and specific heat for PCM's liquid and solid states in the experimental results (Table 6) as reported by Fuentes et al. [23].

$$E_{impregnated\ wood} = x \cdot E_{PCM} + (1 - x) \cdot E_w \quad (5)$$

$$x = \frac{V_{PCM}}{V_{PCM} + V_w} \quad (6)$$

where $E_{impregnated\ wood}$, $\cdot E_{PCM}$ and E_w are any property of the impregnated wood, PCM, and wood, respectively. The volumes V_{PCM} and V_w correspond to that of PCM and unimpregnated wood, respectively.

Table 6. Experimental thermal properties for predicting them in octadecane-impregnated Pinus radiata wood, using the rule of mixtures.

Thermal property	**Octadecane** [23]	***Pinus radiata*** [23]	**Impregnated Wood** [23]	**Impregnated wood (Rule of mixtures)**	**Relative error**
$\boldsymbol{\rho}$ **[kg/m^3]**	780.0	388.0	836.1	836.1	--
$\mathbf{k_S}$ **[W/mK]**	0.4489	0.3111	0.3255	0.3605	11%
$\mathbf{k_L}$ **[W/mK]**	0.1252	--	0.2185	0.2442	12%
$\mathbf{C_{P,S}}$ **[kJ/m^{3}K]**	3634.4	1141.0	2130.8	2037.0	4%
$\mathbf{C_{P,L}}$	2229.2	--	1361.8	1348.2	1%

$[\mathbf{kJ/m^3K}]$					
$\mathbf{L_F}$ $[\mathbf{kJ/kg}]$	133.2	--	133.2	133.2	--

Additionally, we used Equations (7) and (8) extracted from the work of Vasco et al. [52] to estimate the enthalpy curve as a function of temperature using both the experimental properties of octadecane-impregnated wood and those predicted by the rule of mixtures. Figure 6a shows that both enthalpy curves are close.

$$h = \frac{1}{\overline{\rho}}\left[\overline{C_{p,S}} \cdot (1-\varphi) + \overline{C_{p,L}} \cdot f\right] \cdot T + \frac{W_{PCM}}{W_{impregnated\ wood}} \cdot L_F \cdot \varphi \qquad (7)$$

$$\varphi = \begin{cases} 0 & \text{if } T < T_{pc} \\ 1 & \text{if } T \geq T_{pc} \end{cases} \qquad (8)$$

where $\overline{\rho}$ is the apparent average density of impregnated wood, $\overline{C_{p,S}}$ and $\overline{C_{p,L}}$ are the volumetric heat capacity of impregnated wood with solid and liquid PCM, respectively. $W_{PCM}/W_{impregnated\ wood}$ is the PCM mass and impregnated wood mass ratio. L_F is the phase change enthalpy, T_{pc} is the phase change temperature, and φ is the liquid fraction of the PCM used.

The PCMs used to estimate the properties of impregnated wood are those that are made commercially available by PureTemp® [53], which are fatty oils of natural origin and an environmentally friendly alternative to petroleum-based paraffin. The thermal properties of the selected biobased PCMs (Table 7) and the rules of mixtures allow obtaining the thermo-physical properties of impregnated wood (Table 8).

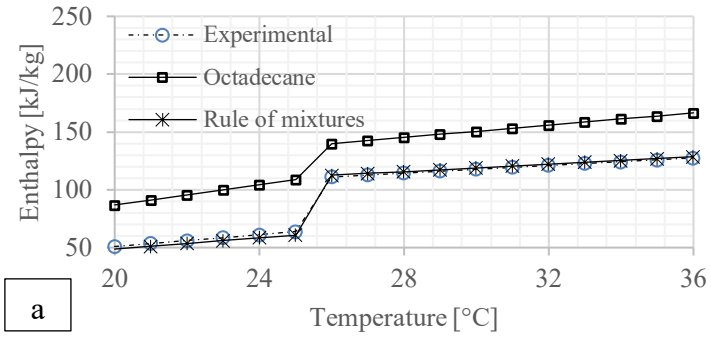

478

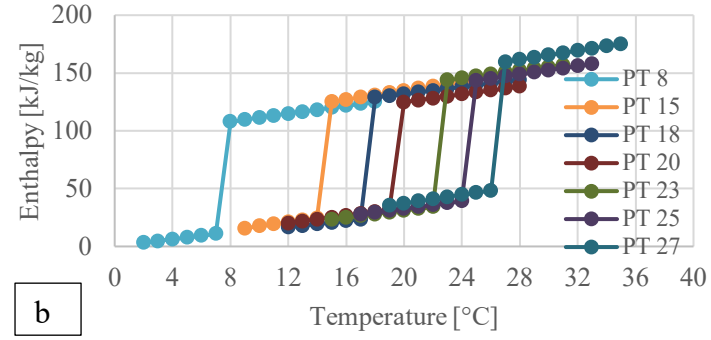

479

480 *Figure 6. Enthalpy-temperature curves of octadecane and octadecane-impregnated Pinus*
481 *radiata wood using experimental data* [23] *and the rule of mixture (a). Enthalpy-temperature*
482 *curves of PureTemp® impregnated Pinus radiata wood calculated with the rule of mixture (b).*

483 Table 7. Thermo-physical properties of PureTemp® bio-based PCMs [53].

PCM	ρ_L [kg/m^3]	ρ_S [kg/m^3]	k_L [W/mK]	k_S [W/mK]	$C_{P,L}$ [kJ/m^{3}K]	$C_{P,S}$ [kJ/m^{3}K]	L_F [kJ/kg]
PT 8	860	950	0.14	0.22	2.15	1.85	187
PT 15	860	950	0.15	0.25	2.56	2.25	182
PT 18	860	950	0.15	0.25	1.74	1.47	192
PT 20	860	950	0.14	0.23	2.15	2.07	171
PT 23	830	910	0.15	0.25	1.99	1.84	201

PT 25	860	950	0.15	0.25	2.29	1.99	187
PT 27	860	950	0.15	0.25	2.63	2.46	202

484 *Table 8. Estimated thermophysical properties of impregnated Pinus radiata wood with different*
485 *PureTemp® PCMs.*

PCM	$\boldsymbol{\rho}$ $[\mathbf{kg/m^3}]$	$\mathbf{k_L}$ $[\mathbf{W/mK}]$	$\mathbf{k_S}$ $[\mathbf{W/mK}]$	$\mathbf{C_{P,L}}[\mathbf{kJ/m^3K}]$	$\mathbf{C_{P,S}}[\mathbf{kJ/m^3K}]$	$\mathbf{L_F}[\mathbf{kJ/kg}]$
PT 8	834.2	0.2495	0.2783	1333.6	1249.5	178
PT 15	834.2	0.2531	0.2891	1448.5	1361.6	182
PT 18	834.2	0.2531	0.2891	1218.7	1143.0	192
PT 20	834.2	0.2495	0.2819	1333.6	1311.2	171
PT 23	834.2	0.2531	0.2891	1288.7	1246.7	201
PT 25	834.2	0.2531	0.2891	1372.8	1288.7	187
PT 27	834.2	0.2531	0.2891	1468.1	1420.5	202

3.5. Optimization parameters

486

487 Genetic algorithms, especially NSGA-II, have gained prominence in optimizing architectural
488 and constructive variables of buildings for design, retrofitting, and refurbishment. Vukadinović
489 et al. [54] compiled a series of studies of building design variables, emphasizing the parameters
490 of different optimization algorithms. Among them are NSGA-II, such as population size, the
491 maximum number of generations, crossover ratio, and mutation probability, which play a role in
492 the algorithm and depend mainly on each optimization problem. The maximum number of
493 generations ranges between 25 and 200, 100 being the most common. The population size
494 varies between 20 and 64, and the crossover rate ranges between 0.7 and 0.95, 0.9 being the
495 most commonly used value. Lei and Shan [59] also recommend that the crossover rate should
496 range between 0.4 and 0.99. The mutation rate controls the frequency of the mutation gene

497 operation. Lei and Shan [55] recommend a range between 0.0001 and 0.1. The tournament size
498 is the size of a random sample taken from the current generation and selects better solutions
499 from the current generation. In this case, we used the default value of the Design-Builder
500 software. On the other hand, Ascione et al. [56] recommend values of the population size from 2
501 to 6 times the number of design variables. According to the above, Table 9 shows the
502 parameters configured for the NSGA-II multi-objective optimizations.

503 *Table 9. Configuration of the NSGA-II parameters.*

NSGA–II Parameter	Value
Maximum number of generations	100
Initial population size	30
Tournament size	2
Crossover rate	0.9
Mutation probability	0.3

4. Results and discussion

504
505 This section details Steps 7–10 of the proposed methodology. Specifically, we present and
506 analyze the optimization results by forming groups according to the typical characteristics of the
507 Pareto solutions. Moreover, we chose a Pareto solution to continue with the analysis proposed
508 in our methodology.

4.1. Optimization results

509
510 The NSGA–II optimization process gave place to 21 optimal retrofit options, constituting the
511 Pareto front. Figure 7a shows all of the feasible solutions and the Pareto front, and Figure 7b
512 shows the Pareto front remarking in green one Pareto point, which is worth analyzing in detail,
513 as it corresponds to the solution with the lower distance to the UP, obtained throughout the

interception of the vertical and horizontal dashed lines in the exact figure. These vertical and horizontal dashed lines intercept the Pareto solutions corresponding to the minimum electricity consumption (ME) and minimum discomfort hours (MD). The base case gives values for the energy consumption and discomfort hours of 13247.92 kWh and 6182.4 hours, respectively. Regarding these values, we calculated the electricity consumption and discomfort hours reductions for each Pareto solution (Figure 8). The reductions in discomfort hours vary between 18.8% and 21.7%; the reductions in electricity consumption vary between 76.4% and 80.5%, with average reduction values of 20.4 ± 1.0% and 78.7 ± 1.2%, respectively.

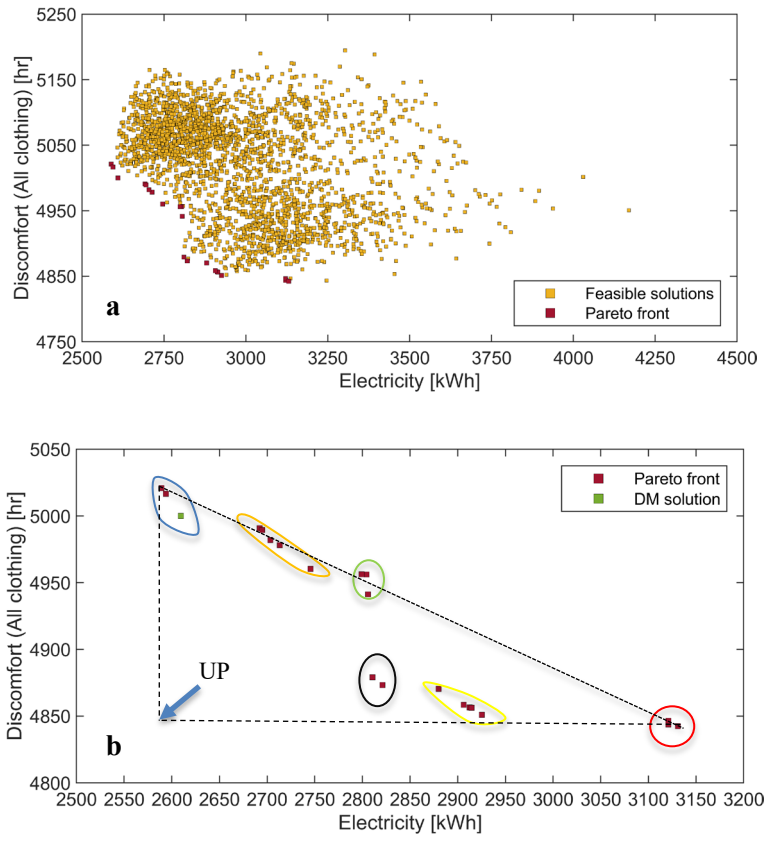

Figure 7. The balance between the two opposing objective functions: discomfort hours and electricity for cooling and heating (a) and Pareto front with the optimal points classified according to different groups(b).

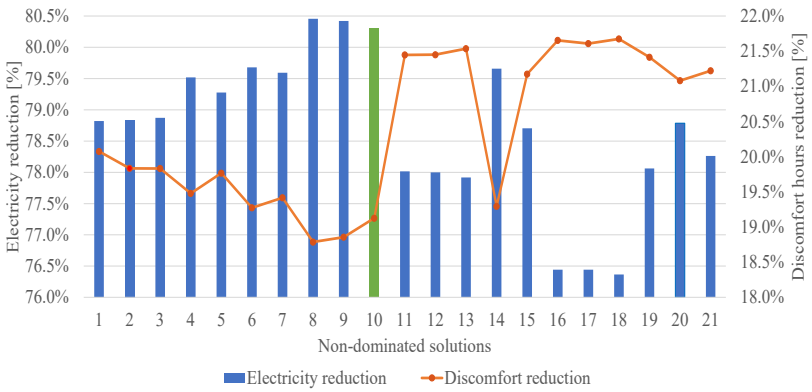

Figure 8. Reduction of electricity consumption and thermal discomfort hours of the 24 non-dominated solutions.

Figure 9 presents the distribution of PF insulation thickness in the three retrofitted walls of the house. For M1 (west-facing), the non-dominated solutions present a higher proportion (76%) of 50 mm thickness PF In M2 (north-facing), most of the non-dominated solutions coincide in not using insulation (67%) even though 33% of the non-dominated solutions predict the use of PF thickness of 50 mm. Finally, most of the non-dominated solutions (90%) predict a PF-layer thickness of 85 mm for the east-facing wall (M3).

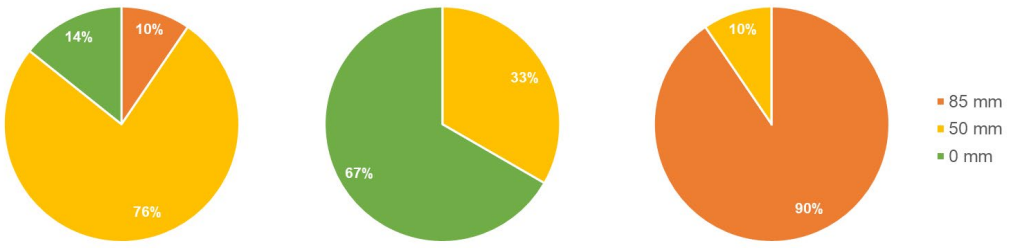

M1 *M2* *M3*

Figure 9 Thickness distribution of polyester fiber (mm) insulation in walls M1, M2, and M3 for the 24 non-dominated solutions.

Regarding the thickness of PCM-impregnated *Pinus radiata* wood (SSPCM-W), the solution's distribution is broad (Figure 10). For M1 (west-facing), the non-dominated solutions present an

equal proportion (24%) for impregnated wood-layer thicknesses of 8 and 12 mm, whereas, minor fractions of 19, 14, and 10% correspond to 5 and 18, and 5 and 10 mm thicknesses, respectively. In the north-facing wall (M2), most of the non-dominated solutions (33%) correspond to an impregnated wood-layer thickness of 18 mm, followed by 10 mm (29%), 15 and 5 mm (14%), and 12 mm with 10%. Finally, for the east-facing wall (M3), the thicknesses of 18, 15, 12, and 10 are represented by the same percentage (19%) converged, followed by wood layers of 5 mm (14%) and 8 mm (10%).

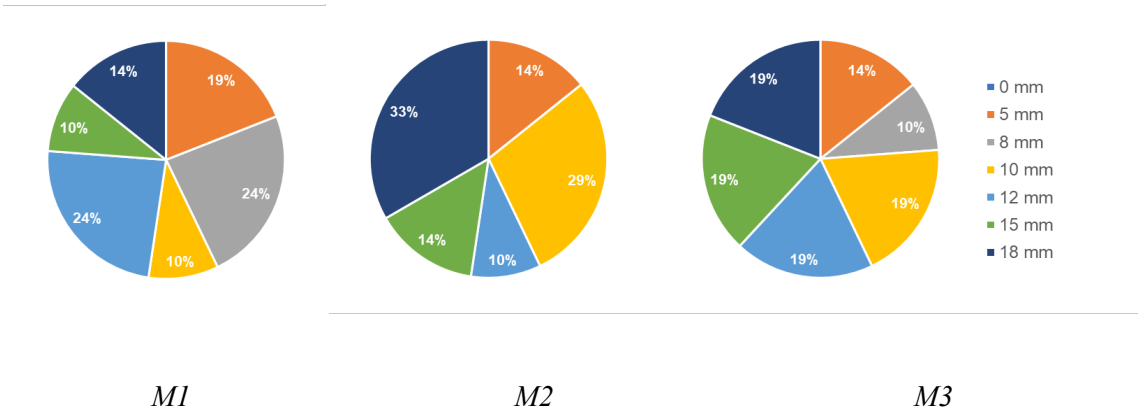

Figure 10. Distribution of the PCM-impregnated wood-layer thickness (mm) in walls M1, M2, and M3 for the 24 non-dominated solutions.

Figure 11 shows the distribution of the wood layer impregnated with PCMs in the retrofitted walls. For the west-facing wall (M1), most of the non-dominated solutions (57%) coincide with using P.T. 27, following the options of P.T. 25 (19%), P.T. 23, and P.T. 20 (10%), and P.T. 8 is the less common option with 8%. In wall M2 (north-facing), the non-dominated solutions correspond mainly to P.T. 25, P.T. 27, and P.T. 23 with 48% and 38%, and 14%, respectively. For the east-facing wall, most of the non-dominated solutions (95%) coincide in using an impregnated wall with P.T. 23, and 5% predict the use of P.T. 25. It must be noted how none of the non-dominated solutions predict using non-impregnated wood in the retrofitted walls.

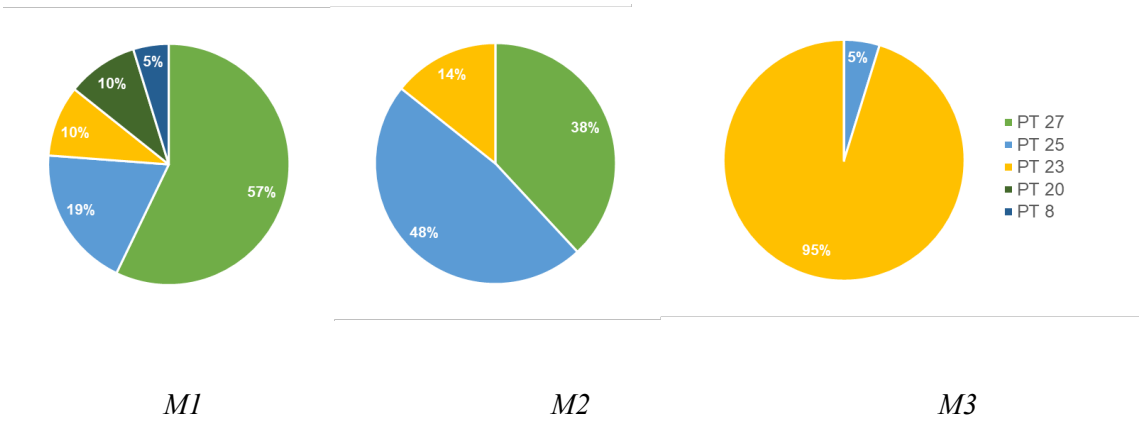

Figure 11. Distribution of commercial PT PCM types in walls M1, M2, and M3 for the 24 non-dominated solutions.

Konstantinidou et al. [57] evaluated the impact of gypsum panels with microencapsulated PCM on the envelope of a 144 m^2 office building in Athens (Greece), which has the same Köppen climate classification as Santiago de Chile, Csa. The authors conducted a multi-objective optimization with NSGA-II, minimizing the cooling loads and the thermal discomfort hours. They found that all of the non-dominated solutions include a PCM with a melting temperature of 22 °C in the south wall. These results are similar to those of our study where the melting temperature was found to be 23–27 °C. Further, Soares et al. [58] found more significant energy savings in warmer climates due to PCMs incorporation (about 55%). Thus, optimum thickness of the PCM-enhanced gypsum board was achieved when its thickness was 40 mm more than was the case with our findings, as depicted in Figure 10, for the same melting temperature.

Regarding the type and thickness of the thermal insulation in the ceiling, almost all of the non-dominated solutions (95%) coincide when using a glass wool layer of 80 mm, which is less than what was determined by Carreras et al. [59], i.e., 110 mm. Finally, regarding the type of windows, all of the non-dominated solutions require the use of double-glazed windows of 3 mm glass thickness with 13 mm spacing (2.716 [$W/(m^2 \cdot °C)$]).

Figure 7b shows the Pareto solutions classified into six groups, with four crossed by the line corresponding to the lower electricity consumption and lower discomfort hours (reference line).

The other two groups are between the reference line and horizontal and vertical lines whose interception gives place to UP. Table 10 tabulates the common characteristics shared by the optimal points of each group. According to their position in the reference line, groups blue and red are opposite. The optimal points of the blue group have better thermal insulation than those of the red group. The orange group's optimal points have thermal insulation similar to those of the blue group, but the wood layers are thicker in the former group. The green group's optimal points are a combination of those of the blue and red groups, thermally insulated in the M1 and M3 walls and without thermal insulation in the M2 wall. The black and yellow groups out of the line share several characteristics even though the range of the wood-layer thickness of the yellow group is more than the black one.

Table 10. Shared characteristics of the optimal points. The classification corresponds to the group colors in Figure 7b.

Group (Optimal points)	**Characteristic**	**M1 West-facing**	**M2 North-facing**	**M3 East-facing**
Blue (3)	PF layer	50 mm	50 mm	85 mm
	T_{pc}	23 and 25 °C	23 °C	23 °C
	SSPCM-W layer	--	10 and 15 mm	10 and 12 mm
Orange (5)	PF layer	50 mm	50 mm	85 mm
	T_{pc}	20 and 23 °C	25 °C	23 °C
	SSPCM-W layer	-	18 mm	12 and 18 mm
Green (3)	PF layer	85 and 50 mm	No insulation	50 and 85 mm
	T_{pc}	--	23 °C	23 and 25 °C
	SSPCM-W layer	--	15 and 18 mm	8 and 10 mm
Red (3)	PF layer	No insulation	No insulation	85 mm

	T_{pc}	25 and 27 °C	25 and 27 °C	23 °C
	SSPCM-W layer	10 and 12 mm	12 and 15 mm	--
Black (2)	PF layer	50 mm	No insulation	85 mm
	T_{pc}	23 °C	25 °C	23 °C
	SSPCM-W layer	--	18 mm	5 mm
Yellow (5)	PF layer	50 mm	No insulation	85 mm
	T_{pc}	23 and 25 °C	25 °C	23 °C
	SSPCM-W layer	--	--	--

4.2. Analysis of the chosen optimal results

This analysis focuses on three optimal points of the Pareto front: the points with the MD and ME, and the point that meets the criteria of minimum distance to UP, i.e., the DM point. Table 11 present the constructive characteristics of the selected optimal points. According to the optimal MD, the house does not need thermal insulation in the west and north-facing walls, but these walls would require a PCM with a higher melting temperature. Regarding the same walls, the optimal solutions ME and DM are similar, presenting differences between the melting temperatures of the PCMs used in the west-facing wall and the thickness of the impregnated wood layer. Regarding the east-facing wall, the three optimal solutions coincide with using the same thickness of PF, the same melting temperature of the PCM used, but different layer thicknesses of impregnated wood. The three optimal solutions for the ceiling and windows required the same choices.

604 *Table 11. Characteristics of the retrofitted solutions for the selected optimal points.*

Optimal point	Characteristic	M1 West-facing	M2 North-facing	M3 East-facing	Ceiling	Windows
Minimum electricity consumption (ME)	PF layer	50 mm	50 mm	85 mm	Glass wool 80 mm	Double glazed 3 mm thickness/13 mm spacing
	T_{pc}	23 °C	23 °C	23 °C		
	SSPCM-W layer	12 mm	15 mm	15 mm		
Decision maker (DM)	PF layer	50 mm	50 mm	85 mm		
	T_{pc}	25 °C	23 °C	23 °C		
	SSPCM-W layer	18 mm	10 mm	12 mm		
Minimum discomfort hours (MD)	PF layer	--	--	85 mm		
	T_{pc}	27 °C	27 °C	23 °C		
	SSPCM-W layer	12 mm	10 mm	10 mm		

605 The passive analysis considers the variation in comfort hours regarding the base case of the
606 three optimal points during the year (Figure 12). The living and dining room (Figure 12a)
607 presents an overall reduction in discomfort hours during the year, especially during the spring
608 and autumn seasons. It is interesting to notice that the optimal point, ME presents better thermal
609 comfort conditions under a passive scenario. Regarding Bedroom 1 (Figure 12b), which is west-
610 facing, the thermal comfort improves during winter, ranging from 14.8 to 18.4%. The
611 improvement in thermal comfort during spring improves slightly with values of less than 1%.
612 During summer and autumn, the hours of discomfort hours increase by 11.6 and 3.4% on
613 average, respectively. The east-oriented Bedrooms 2 (Figure 12c) and 3 (Figure 13 c) show an
614 increase in thermal discomfort hours during the year, especially during the year's warmer

seasons. During winter, the increase in thermal discomfort hours is lower than 2.5% and 10% for Bedrooms 2 and 3, respectively. It is interesting to notice how under a passive scenario, the optimal results give place to a thermal comfort improvement in the dwelling's zone with the highest occupation rate, i.e., the living and dining room. Moreover, the higher rise in thermal discomfort hours occurs during the warmer seasons in the east-facing bedrooms. Therefore, even under a passive scenario, the retrofitted dwelling may provide better comfort conditions to the dwelling's inhabitants.

Figure 13 shows the heating and cooling energy consumption variation over a year for the three chosen optimal points. The optimal point of MD presents higher heating and cooling demands than the optimal point with ME and the DM point. Regarding the heating consumption, the difference between the optimal solutions ME and DM does not exceed 1% during winter, even though the optimal solution MD presents a higher heating demand of 25.2% on average. The cooling consumption of the optimal points DM and ME are pretty similar during summer but, on average, 20% higher than the optimal point MD.

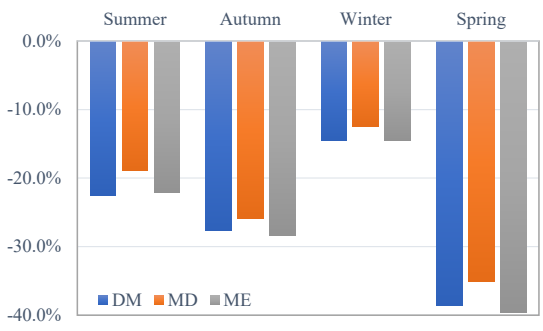

(a) Living and dining room

(b) Bedroom 1

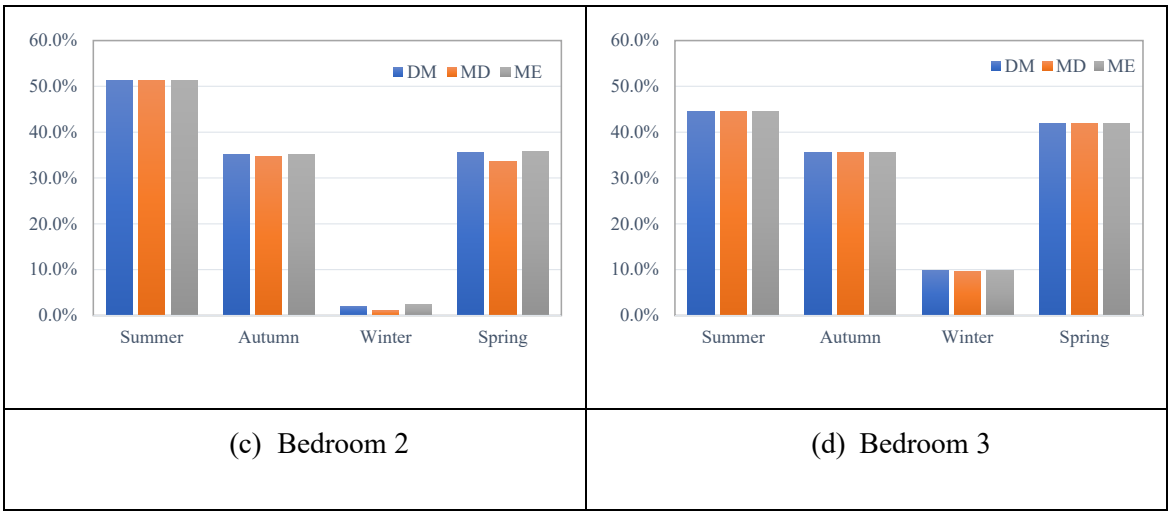

Figure 12. Variation in comfort hours regarding the base case of the optimized dwelling. Minimum discomfort hours (MD), minimum electricity consumption (ME), and decision maker (DM) optimal point.

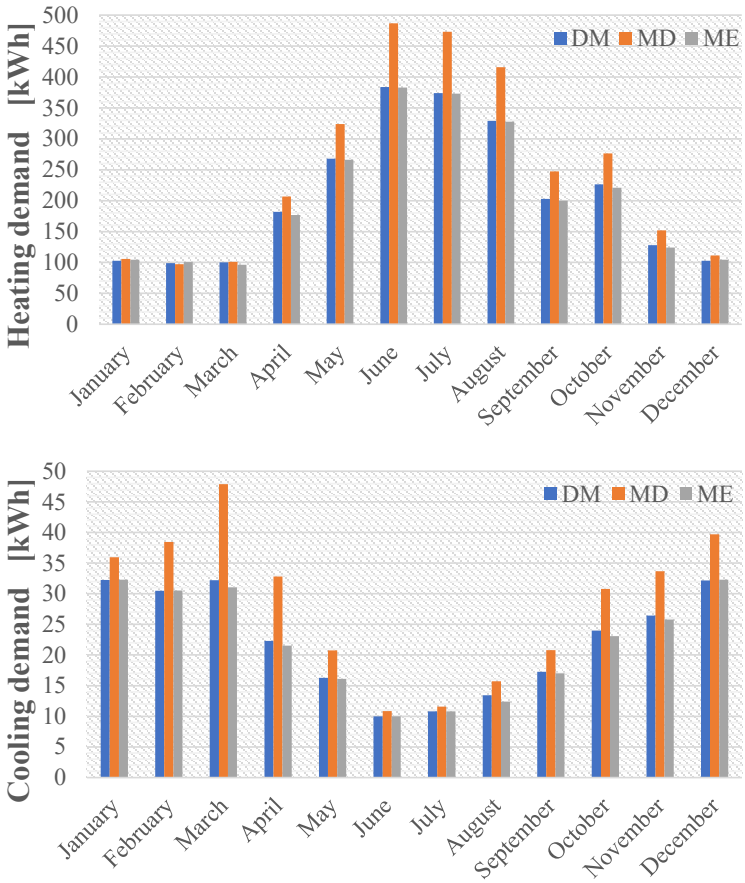

Figure 13. Heating and cooling energy consumption of the optimized dwelling during the year. Minimum discomfort hours (MD) and minimum electricity consumption (ME), and decision maker (DM).

Table 12 shows the obtained electricity consumption values per conditioned building area of the optimized dwelling. Generally, the heating demand is one order of magnitude greater than the cooling demand for the three optimal points, and the heating and cooling demand per conditioned building area for the optimal DM is only 0.77% and 4.20% higher than the optimal ME values. Regarding thermal comfort, a decrease of only 3.6% in thermal discomfort hours, which is the difference between the optimal points MD and DM, requires an increase of 21% and 32% in heating and cooling demand, respectively.

Finally, let us compare the results of Table 12 with Table 4 for the base case. We find that the retrofitting optimization of the dwelling envelope reduces the heating and cooling electricity consumption per conditioned building area by 5 and 10 times, respectively.

Table 12 Energy consumption per conditioned building area of the optimized dwelling. Minimum discomfort hours (MD), minimum electricity consumption (ME), and decision maker (DM) optimal point.

Zone	**Heating [kWh/(m^2·year)]**			**Cooling [kWh/(m^2·year)]**		
	DM	MC	ME	DM	MC	ME
Bedroom 1	40.35	61.51	39.91	4.22	8.09	4.14
Bedroom 2	46.93	58.11	46.45	3.30	3.68	3.28
Bedroom 3	26.50	26.26	26.39	3.56	3.59	3.55
Living and dining room	46.40	49.02	46.14	5.56	5.96	5.16

Dwelling	41.59	49.93	41.27	4.46	5.65	4.28

4.3. Economic analysis

To analyze the technical-economic feasibility of the decision–maker's optimal solution for the housing typology of the Metropolitan region, we used economic indexes such as the PNV, IRR, and PBP. The optimized dwelling is in the Municipality of Macul, where the electricity consumption is composed of three parts: a fixed monthly charge of USD 0.75, the second one is a charge for the transport of electricity, which amounts to 0.014 USD/kWh, and the third one consists of a charge for electricity consumed of 0.12 USD/kWh. Therefore, given that the annual electricity savings by implementing the DM optimal solution are 13,140.44 kWh, the annual savings amount to USD 1,712.7 (Table 13).

Table 13. Annual electricity consumption of the decision maker's optimal solution and the base case.

Annual electricity consumption		**Cost [USD]**
Base case [kWh]	15,905.33	2,082.03
DM optimal [kWh]	2,764.89	369.33
Savings [kWh]	13,140.44	1,712.7

On the other hand, to estimate the cost of *Pinus radiata* wood layers with PCM, we used the price per pound of PCM from the supplier PureTemp [53], which is 2–5 USD/pound. Equation (9) allows calculating the price of the layers of wood impregnated with PCM for each wall,

$$P_{W-PCM} = (A_W \cdot P_W + Q_{PCM} \cdot P_{PCM}) \cdot 1.36 \quad (9)$$

where the constant 1.36 has been obtained from the average price increase of *Pinus radiata* lumber when impregnated with Chromated copper arsenate is 36% in the national market, P_{W-PCM} is the price of the wood layer impregnated with PCM for each wall; A_W and P_W are the

area of the wood layer and the price per unit area, respectively. Q_{PCM} corresponds to the mass of PCM required for each wall and P_{PCM} is the PCM price per kilogram. Table 14 shows the quantities and prices of the materials that make up each wood layer impregnated with PCM for the three intervened walls. Even though leakage and thermal stability of SSPCMs are vital issues, a consideration of these aspects is beyond the scope of this work. Leakage has been identified as an issue in several studies of SSPCM based on wood, showing that PCM viscosity, PCM load, and the wood species are relevant parameters [51]. Assuming that the leakage issue would be overcome, according to the PCM manufacturer, PureTemp, PCMs do not experience thermal degradation when exposed to over 65,000 thermal cycles [60], which implies that PCMs can endure up to 7 thermal cycles per day during the project. Therefore, we assume that the SSPCM-wood panels are stable during the payback period. Table 15 presents the other required materials incorporated into the thermal envelope of the dwelling. Despite the high investment for retrofitting shown in Table 15, the Chilean Housing and Neighborhood Improvement Program would fund 55% of the materials investment, including thermal insulation and windows.

Table 14. Quantity and price of PCM-impregnated wood layer materials used for the three walls.

Wall	$\mathbf{A_W\ [m^2]}$	$\mathbf{P_W\ [USD/m^2]}$	$\mathbf{Q_{PCM}\ [kg]}$	$\mathbf{P_{W-PCM}\ [USD]}$
M1	10.21	11.74	161.58	2,999.95
M2	17.50	9.14	153.91	2,919.60
M3	13.3	10.00	140.39	2,645.78

For the calculation of the PNV and the PBP, the discount rate is the opportunity cost of not dedicating the funds of the initial investment in adjustable savings account with profitability of U.F. + 0.1%, which considering the average inflation of the last two years, results in a discount rate of 3.1%. The above added to a project horizon of 25 years, as suggested by the study of

Hernandez et al. [61], results in a PNV of USD 5,453.63, an IRR of 5.04%, and a PBP of 12.9 years.

Table 15. Quantity and price of other materials required for the decision maker's optimal solution.

Material	Quantity [m^2]	USD/m^2	Total (USD)
PF 85 mm	13.3	2.87	38.26
PF 50 mm	27.7	1.41	39.02
Glass wool 80 mm	145.6	2.88	418.78
Plasterboard 10 mm	406.7	2.10	853.20
Windows	--	--	2,177.34
Wood-PCM 25 18 mm	10.21	--	2,999.95
Wood-PCM 23 10 mm	17.50	--	2,919.60
Wood-PCM 23 12 mm	13.3	--	2,645.78
HVAC Systems	--	--	1,633.00
Installation		--	10,315.33
		Total	**22,040.26**

Conclusion

This work presents a methodology to find the optimum configuration of different passive constructive variables, especially the incorporation of *Pinus radiata* wood panels impregnated with PCMs in the thermal envelope. This methodology can help retrofit low-income dwellings that do not meet the requirements of the thermal regulations. In the presented study, we applied it to a housing typology in the Metropolitan Region of Chile. The calibration of the typology

allowed us to identify a low thermal performance situation, where the thermal discomfort hours and the rate of infiltration were both high, a situation that is common in the existing houses in Chile that were built before 2008. The active analysis of the housing typology found an energy demand intensity for heating and cooling of 201.3 kWh/(m^2/year) and 45.4 kWh/(m^2/year), respectively. These values can potentially reduce to 41.6 kWh/(m^2/year) for heating and 4.5 kWh/(m^2/year) for cooling, respectively, by incorporating an optimized retrofitting solution. The results of the economic analysis that was carried for the retrofitting solution suggest that despite the high investment required for incorporating PCMs in the thermal envelope, its payback period of 12.9 years is reasonable.

Acknowledgments

The authors would like to acknowledge Fondecyt 1201520, ANID-Chile, and the Spanish Ministry of Economy and Competitiveness (RTI2018-093849-B-C33, MINECO/FEDER, U.E.). D. Vasco thanks “Fundación Carolina: Programa Estancias Cortas Postdoctorales 2021” for the support in the research stay at University Rovira I Virgili.

References

[1] IEA, "World energy balances." [Online]. Available: https://www.iea.org/data-and-statistics/data-product/world-energy-balances. [Accessed: 03-Aug-2022].

[2] M. Roser, "Economic Growth," *Our World Data*, 2013.

[3] Oficina de Cambio Climático de la Sección de Climatología de and Chile, "Reporte anual de la evolución del clima en Chile," Santiago de Chile, 2021.

[4] "Tercer Informe Bienal de Actualización de Chile sobre Cambio Climático," Santiago de Chile, 2018.

[5] Comisión nacional de energía, "Balance nacional de energía."

[6] C. D. D. TECNOLÓGICO, "Informe Final Uso de la Energía Hogares Chile," 2019.

[7] "Calificación energética de viviendas." [Online]. Available: https://www.eechile.cl/calificacion-energetica-vivienda/. [Accessed: 07-Jun-2022].

[8] A. Cortes and B. Rismanchi, "Residential energy efficiency in Chile. Policies to reduce firewood dependency," *Estoa*, vol. 9, no. 17, pp. 57–68, Jan. 2020.

[9] S. Mirrahimi, M. F. Mohamed, L. C. Haw, N. L. N. Ibrahim, W. F. M. Yusoff, and A. Aflaki, "The effect of building envelope on the thermal comfort and energy saving for high-rise buildings in hot–humid climate," *Renew. Sustain. Energy Rev.*, vol. 53, pp. 1508–1519, 2016.

[10] K. Ulgen, "Experimental and theoretical investigation of effects of wall's thermophysical properties on time lag and decrement factor," *Energy Build.*, vol. 34, no. 3, pp. 273–278, 2002.

[11] R. Parameshwaran, S. Kalaiselvam, S. Harikrishnan, and A. Elayaperumal, "Sustainable thermal energy storage technologies for buildings: A review," *Renew. Sustain. Energy Rev.*, vol. 16, no. 5, pp. 2394–2433, 2012.

[12] M. N. Sánchez, E. Giancola, E. Blanco, S. Soutullo, and M. J. Suárez, "Experimental Validation of a Numerical Model of a Ventilated Façade with Horizontal and Vertical Open

740 Joints," *Energies*, vol. 13, no. 1, 2020.

741 [13] R. Saxena, D. Rakshit, and S. C. Kaushik, "Phase change material (PCM) incorporated
742 bricks for energy conservation in composite climate: A sustainable building solution," *Sol.*
743 *Energy*, vol. 183, pp. 276–284, 2019.

744 [14] Q. Al-Yasiri and M. Szabó, "Incorporation of phase change materials into building
745 envelope for thermal comfort and energy saving: A comprehensive analysis," *J. Build. Eng.*,
746 vol. 36, p. 102122, 2021.

747 [15] M. Frigione, M. Lettieri, and A. Sarcinella, "Phase Change Materials for Energy
748 Efficiency in Buildings and Their Use in Mortars," *Materials (Basel).*, vol. 12, no. 8, 2019.

749 [16] J. Kośny, *PCM-Enhanced Building Components*. Springer Cham, 2015.

750 [17] D. Mathis, P. Blanchet, V. Landry, and P. Lagière, "Impregnation of Wood with
751 Microencapsulated Bio-Based Phase Change Materials for High Thermal Mass Engineered
752 Wood Flooring," *Appl. Sci.*, vol. 8, no. 12, 2018.

753 [18] V. Fernández, C. Valderrama-Ulloa, F. Rouault, C. Schmitt, R. Del Río, and D. Vasco,
754 "Thermal and Mechanical Analysis of Plywood Boards Thermally Enhanced with Phase
755 Change Materials," in *IOP Conference Series: Earth and Environmental Science*, 2020, vol.
756 503, no. 1.

757 [19] C. Barreneche, J. Vecstaudza, D. Bajare, and A. I. Fernandez, "PCM/wood composite
758 to store thermal energy in passive building envelopes," *IOP Conf. Ser. Mater. Sci. Eng.*, vol.
759 251, p. 012111, Oct. 2017.

760 [20] A. Temiz, G. Hekimoğlu, G. Köse Demirel, A. Sarı, and M. H. Mohamad Amini,
761 "Phase change material impregnated wood for passive thermal management of timber
762 buildings," *Int. J. Energy Res.*, vol. 44, no. 13, pp. 10495–10505, 2020.

763 [21] Y. Zhao *et al.*, "Hierarchically channel-guided porous wood-derived shape-stabilized
764 thermal regulated materials with enhanced thermal conductivity for thermal energy storage,"
765 *Mater. Res. Express*, vol. 6, no. 11, p. 115515, Oct. 2019.

766 [22] L. Ma, Q. Wang, and L. Li, “Delignified wood/capric acid-palmitic acid mixture stable-
767 form phase change material for thermal storage,” *Sol. Energy Mater. Sol. Cells*, vol. 194, pp.
768 215–221, 2019.

769 [23] R. Fuentes-Sepúlveda, C. García-Herrera, D. A. Vasco, C. Salinas-Lira, and R. A.
770 Ananías, “Thermal Characterization of Pinus radiata Wood Vacuum-Impregnated with
771 Octadecane,” *Energies*, vol. 13, no. 4, 2020.

772 [24] C. Montanari, Y. Li, H. Chen, M. Yan, and L. A. Berglund, “Transparent Wood for
773 Thermal Energy Storage and Reversible Optical Transmittance,” *ACS Appl. Mater. Interfaces*,
774 vol. 11, no. 22, pp. 20465–20472, Jun. 2019.

775 [25] X. Lin *et al.*, “Fabrication of thermal energy storage wood based on graphene aerogel
776 encapsulated polyethylene glycol as phase change material,” *Mater. Res. Express*, vol. 7, no. 9,
777 p. 95503, Sep. 2020.

778 [26] J. U. Hartig, F. Hilkert, J. Wehsener, and P. Haller, “Potential of reducing energy
779 consumption in timber buildings by impregnation of wood with phase-change materials,” in
780 *World Conference on Timber Engineering 2021, WCTE 2021*, 2021.

781 [27] M. Alam, H. Jamil, J. Sanjayan, and J. Wilson, “Energy saving potential of phase
782 change materials in major Australian cities,” *Energy Build.*, vol. 78, pp. 192–201, Aug. 2014.

783 [28] H. Wang, W. Lu, Z. Wu, and G. Zhang, “Parametric analysis of applying PCM
784 wallboards for energy saving in high-rise lightweight buildings in Shanghai,” *Renew. Energy*,
785 vol. 145, pp. 52–64, 2020.

786 [29] S. N. Al-Saadi and Z. (John) Zhai, “A new validated TRNSYS module for simulating
787 latent heat storage walls,” *Energy Build.*, vol. 109, pp. 274–290, 2015.

788 [30] J. Bohórquez-Órdenes, A. Tapia-Calderón, D. A. Vasco, O. Estuardo-Flores, and A. N.
789 Haddad, “Methodology to reduce cooling energy consumption by incorporating PCM
790 envelopes: A case study of a dwelling in Chile,” *Build. Environ.*, vol. 206, p. 108373, 2021.

791 [31] S. Ramakrishnan, X. Wang, J. Sanjayan, and J. Wilson, “Thermal performance of

792 buildings integrated with phase change materials to reduce heat stress risks during extreme
793 heatwave events," *Appl. Energy*, vol. 194, pp. 410–421, 2017.

794 [32] J. Lee and J. Park, "Phase Change Material (PCM) Application in a Modernized Korean
795 Traditional House (Hanok)," *Sustainability* , vol. 10, no. 4. 2018.

796 [33] S. N. Murray, B. P. Walsh, D. Kelliher, and D. T. J. O'Sullivan, "Multi-variable
797 optimization of thermal energy efficiency retrofitting of buildings using static modelling and
798 genetic algorithms – A case study," *Build. Environ.*, vol. 75, pp. 98–107, 2014.

799 [34] D. Gossard, B. Lartigue, and F. Thellier, "Multi-objective optimization of a building
800 envelope for thermal performance using genetic algorithms and artificial neural network,"
801 *Energy Build.*, vol. 67, pp. 253–260, 2013.

802 [35] E. Asadi, M. G. da Silva, C. H. Antunes, L. Dias, and L. Glicksman, "Multi-objective
803 optimization for building retrofit: A model using genetic algorithm and artificial neural network
804 and an application," *Energy Build.*, vol. 81, pp. 444–456, 2014.

805 [36] "ReNaM." [Online]. Available: https://renam.cl/. [Accessed: 05-May-2022].

806 [37] "Censo 2017." [Online]. Available: http://www.censo2017.cl/. [Accessed: 14-Jun-
807 2022].

808 [38] "Encuesta Casen 2017." [Online]. Available:
809 http://observatorio.ministeriodesarrollosocial.gob.cl/encuesta-casen-2017. [Accessed: 14-Jun-
810 2022].

811 [39] "Permisos de edificación." [Online]. Available:
812 https://www.ine.cl/estadisticas/economia/edificacion-y-construccion/permisos-de-edificacion.
813 [Accessed: 14-Jun-2022].

814 [40] "Encuesta Casen 2015." [Online]. Available:
815 http://observatorio.ministeriodesarrollosocial.gob.cl/encuesta-casen-2015. [Accessed: 14-Jun-
816 2022].

[41] A. Yáñez, Cristián; Fissore, Adelqui; Leiva, “Informe Final Uso de la Energía Hogares Chile 2018,” Santiago de Chile, 2019.

[42] M. de V. y Urbanismo, *Decreto 49: Aprueba Reglamento del Programa Fondo Solidario de Elección de Vivienda*. Santiago de Chile, Chile: Biblioteca del Congreso Nacional de Chile, 2011.

[43] “Programa de Mejoramiento de Viviendas y Barrios.” [Online]. Available: https://www.minvu.gob.cl/beneficio/vivienda/programa-de-mejoramiento-de-viviendas-y-barrios-proyectos-eficiencia-energetica-e-hidrica-para-la-vivienda/. [Accessed: 12-May-2022].

[44] “CARTOGRAFIA DIGITAL SII MAPAS.” [Online]. Available: https://www4.sii.cl/mapasui/internet/#/contenido/index.html. [Accessed: 12-May-2022].

[45] M. División Técnica de Estudio y Fomento Habitacional - Ditec, Ed., *Estándares de construccion sustentable para viviendas de Chile - Tomo II*, Second edi. Santiago de Chile, 2018.

[46] “Desing Builder Chile.” [Online]. Available: https://www.designbuilder.cl/descargas/archivos-climaticos/. [Accessed: 05-Jun-2022].

[47] M. Trebilcock, “Manual de Hermeticidad al Aire de Edificaciones,” Concepción.

[48] A. N. S. Institute, R. of Heating, and A.-C. Engineers, *Thermal Environmental Conditions for Human Occupancy: ANSI/ASHRAE 55-1981*. American Society of Heating, Refrigerating, and Air-Conditioning Engineers, Incorporated, 1981.

[49] Y. Lin and W. Yang, “Application of Multi-Objective Genetic Algorithm Based Simulation for Cost-Effective Building Energy Efficiency Design and Thermal Comfort Improvement,” *Front. Energy Res.*, vol. 6, 2018.

[50] S. Madrid, Hernán; Opazo, Felipe; Parada, Óscar; Vera, “Impacto de las infiltraciones de aire en el desempeño energético y térmico de las viviendas,” *EMB Revista de la Construcción*, 2012.

842 [51] J. U. Hartig, F. Hilkert, J. Wehsener, and P. Haller, “Impregnation of wood with a
843 paraffinic phase change material for increasing heat capacity,” *Wood Mater. Sci. \& Eng.*, vol.
844 0, no. 0, pp. 1–10, 2022.

845 [52] D. A. Vasco, C. Salinas-Lira, I. Barra-Reyes, and D. M. Elustondo, “Kinematic
846 characterization of the pressure-dependent PCM impregnation process for radiata pine wood
847 samples,” *Eur. J. Wood Wood Prod.*, vol. 76, no. 5, pp. 1461–1469, 2018.

848 [53] “PureTemp technical and safety data sheets.” [Online]. Available:
849 https://puretemp.com/?p=220. [Accessed: 16-Jun-2022].

850 [54] A. Vukadinović, J. Radosavljević, A. Đorđević, M. Protić, and N. Petrović, “Multi-
851 objective optimization of energy performance for a detached residential building with a
852 sunspace using the NSGA-II genetic algorithm,” *Sol. Energy*, vol. 224, pp. 1426–1444, 2021.

853 [55] Y. Lei and S. Zhang, *MATLAB genetic algorithm toolbox and its application*, Second.
854 Xi’an University of Electronic Science and Technology Press, 2014.

855 [56] F. Ascione, R. F. De Masi, F. de Rossi, S. Ruggiero, and G. P. Vanoli, “Optimization of
856 building envelope design for nZEBs in Mediterranean climate: Performance analysis of
857 residential case study,” *Appl. Energy*, vol. 183, pp. 938–957, 2016.

858 [57] C. A. Konstantinidou, W. Lang, and A. M. Papadopoulos, “Multiobjective optimization
859 of a building envelope with the use of phase change materials (PCMs) in Mediterranean
860 climates,” *Int. J. Energy Res.*, vol. 42, no. 9, pp. 3030–3047, 2018.

861 [58] N. Soares, A. R. Gaspar, P. Santos, and J. J. Costa, “Multi-dimensional optimization of
862 the incorporation of PCM-drywalls in lightweight steel-framed residential buildings in different
863 climates,” *Energy Build.*, vol. 70, pp. 411–421, 2014.

864 [59] J. Carreras, D. Boer, G. Guillén-Gosálbez, L. F. Cabeza, M. Medrano, and L. Jiménez,
865 “Multi-objective optimization of thermal modelled cubicles considering the total cost and life
866 cycle environmental impact,” *Energy Build.*, vol. 88, pp. 335–346, 2015.

867 [60] “PureTemp.” [Online]. Available: https://puretemp.com/?p=330#panel19. [Accessed:

12-May-2022].

[61] H. Hernández, “Economic assessment of energy efficiency investments in dwellings,” *Build. Manag.*, vol. 1, no. 2, pp. 36–45, 2017.